

Role of spin-orbit coupling effects in rare-earth metallic tetra-borides : a first principle study

Ismail Sk^{1,2} and Nandan Pakhira²

¹*Bajkul Milani Mahavidyalaya, Purba Medinipur-721655, West Bengal, India*

²*Kazi Nazrul University, Asansol-713340, West Bengal, India*

We have investigated the electronic structure of rare-earth tetraborides, RB_4 , using first-principle electronic structure methods (DFT) implemented in Quantum Espresso (QE). In this article we have studied hether-to neglected strong spin-orbit coupling (SOC) effects present in these systems on the electronic structure of these system in the non-magnetic ground state. The calculations were done under GGA and GGA+SO approximations using ultrasoft pseudopotentials and fully relativistic ultrasoft pseudopotentials (for SOC case). Perdew-Burke-Ernzerhof generalized gradient approximation (PBE-GGA) exchange-correlation functionals within the linearized plane-wave (LAPW) method as implemented in QE were used. The projected density of states consists of 3 distinct spectral peaks well below the Fermi energy and separated from the continuum density of states around the Fermi energy. The discrete peaks arises due to rare-earth s -orbital, rare-earth $p + B p$ and $B p$ -orbitals while the continuum arises due to hybridized $B p$, rare-earth d orbitals. Upon inclusion of SOC the peak arising due to rare-earth p -orbitals gets split into two peaks corresponding to $j = 0.5$ and $j = 1.5$ configurations. In case of LaB_4 , in the presence of SOC, spin-split $4f$ orbitals contributes to density of states at the Fermi level while the density of states at the Fermi level largely remains unaffected for all other materials under consideration.

PACS numbers:

I. INTRODUCTION

The strong Coulomb correlations present in $3d$ and $4d$ transition metal compounds as well as in $4f$ lanthanides and $5f$ actinides are key to understanding nonvel and exotic properties. The rare earth lanthanides except Pm are good conductors of heat and electricity. Pm is radioactive with very short life and its occurrence in nature is extremely rare. The rare-earth metallic tetra-borides exhibit various valency such as di, tri and tetravalent state [1]. Cerium (Ce) and Terbium (Tb) primarily show tetravalent state where as the other metallic tetraborides mostly show trivalent state [1]. Recently intermediated valance state of Yb between Yb^{2+} and Yb^{3+} is experimentally observed and Kondo interaction is significant in this system [2].

Recent observation of fractional magnetic plateau in TmB_4 and ErB_4 have created lot of interest in these class of materials. Stable magnetization plateau occuring at $1/2$ fraction (of saturation magnetization) and fractional plateaus at $1/7, 1/8, \dots$ etc [3,4]. fractions are similar to the plateaus observed in the Hall resistivity of two dimensional degenerate electron gases subject to a perpendicular magnetic field.

It is interesting to mention that the position of the rare-earth atoms as shown in Fig. 1 forms a two dimensional Archimedian Shastry-Sutherland lattice (SSL) [5]. SSL consisting of localized spin-1/2 is an example of geometrically frustrated system with huge spin degeneracy and the observation of magnetization plateaus is often attributed to this degeneracy. Insulating $SrCu_2(BO_3)$ [6] is a well studied system which can be effectively mapped onto a nearest-neighbour SSL. However in metallic rare-earth tetraborides “localized” spins interacts only

through long range RKKY [7] type of interactions. Hence the mapping of interacting fermionic model onto an effective spin-1/2 models on SSL with nearest neighbour interaction is highly non-trivial [5,8]. Correlated and frustrated systems are of great academic interest as well as they have many potential technological applications like memory device, spintronics, quantum computation etc. [9]. The very first step towards understanding the intriguing thermodynamic and transport properties in these complex systems is to study their electronic band structure. In an earlier work [10] electronic structure of RB_4 (except TmB_4) have been studied using first principle method. However strong atomic spin-orbit coupling effects present in rare-earth atoms have been neglected. Inclusion of SOC for certain systems [R= Yb, Pr, Gd, Tb, Dy] in the mangetic state have been considered and also considered of $4f$ for RB_4 but there is no systematic study of such effects in the non-magnetic (paramagnetic) state [11]. In the present work we make a detailed study of SOC effects on the electronic structure of rare earth tetra-borides. In particular we have chosen systems (R=La, Ce, Nd, Sm) with relatively low SOC effects as well as systems (R=Ho,Er,Tm,Lu) with relatively high SOC effects.

The organization of the rest of the paper is as follows. In Sec. II we discuss crystal structure of the system. In Sec. III we elaborate the computational details for band structure. In Sec. IV we discuss the results for various systems and finally in Sec. V we conclude.

II. CRYSTAL STRUCTURE

RB_4 crystallizes in the tetragonal symmetry with space group $P4/mbm$ [12,13]. Fig. 1 summarizes crystal structure of RB_4 from different perspectives. Fig. 1 (a) displays the full tetragonal structure which consists of alternate layers of rare-earth (R) and B ions stacked along c -axis. Fig. 1(b) shows the top view of the crystal structure. There are two distinct types of B atoms - (i) planar and (ii) octahedral. Boron atoms form octahedra as well as 7-atom rings in the $a-b$ plane [14]. Ring forming planar B atoms (shown in blue) which are not part of octahedra also forms dimers and these dimers are arranged in a regular pattern. In Fig. 1(c) we show one unit cell formed by four such B octahedra. In Fig. 1(d) we show SSL formed by the B atoms. From Fig. 1(b) it is clear that out of the 4 B atoms two are nearer than other two. The exchange interaction between the two near B atoms mimics the nearest neighbour interaction (J) and the interaction between the distant B atoms mimics interaction along alternate diagonals. It is important to mention that B atoms play a crucial role in the electronic structure of these systems as they are in the sp -hybridized state.

III. COMPUTATIONAL DETAILS

First-principle calculations were performed using density functional theory (DFT)[15,16] as implemented in the open source package Quantum Espresso [17] under the Burai [18] framework. The calculations are done within GGA and GGA+SO approximation. We have used Ultra soft pseudo-potentials [19] Marzari- Vanderbilt smearing [20] for structural optimization and total energy calculation of the system. Further, Perdew-Burke-Ernzerhof Generalized Gradient Approximation (PBE-GGA) exchange-correlation functional within the linearized augmented plane wave (LAPW) method is employed [21,22]. For the case with SOC effect full relativistic Ultra soft pseudo-potentials were used. The total Hamiltonian of the Kohn-sham DFT calculations with Spin-Orbit coupling can be written as [23]

$$\hat{H} = \hat{T} + \hat{V}_{ext} + \hat{V}_{es} + \hat{V}_{xc} + \hat{H}^{SOC} = \hat{T} + \hat{V}_a + \hat{H}^{SOC}, \quad (1)$$

where, \hat{T} , \hat{V}_{ext} , \hat{V}_{es} , \hat{V}_{xc} and \hat{H}^{SOC} are the kinetic energy operator, external potential operator, electrostatic or hartree potential operator, exchange-correlation potential operator and spin-orbit coupling operator respectively. \hat{V}_a is the applied field or Kohn-Sham potential operator. The Hamiltonian \hat{H}^{SOC} for relativistic limit in terms of momentum and spin operator can be expressed as [23]

$$\hat{H}^{SOC} = \frac{i}{4c^2} (\nabla \hat{V}_a \times \hat{p}) \cdot \hat{s} \quad (2)$$

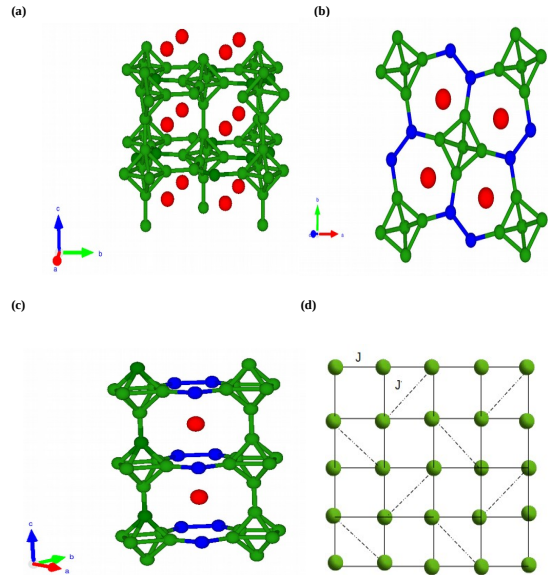


FIG. 1: (Color online) Tetragonal crystal structure of RB_4 . Fig. 1(a) represents the full structure consisting of different layers of rare-earth, R, ions (red) and B (green) stacked along c -axis. (b) Top view of the B sublattice (in the $a-b$ plane) comprising of 7 atom ring and a square formed by the position of the R atoms. (c) Side view of the B sublattice (along c -axis) showing two different types of B ; one forming dimer (shown in blue) and the other part of the B octahedra (shown in green). (d) Shastry-Sutherland lattice in two dimension.

For the central field approximation the Hamiltonian \hat{H}^{SOC} [23] can be written as

$$\hat{H}^{SOC} = \zeta \hat{l} \cdot \hat{s} \quad (3)$$

where \hat{l} is the angular momentum and $\zeta = \frac{1}{2m^2 c^2 r} \frac{dV_a}{dr}$, where c is the speed of light.

The lattice information were taken from the materials research project site [24]. The lattice constants, the kinetic energy cut-off (Ecutwfc) and charge density cut-off (Ecutrho) values used for RB_4 are mentioned in Table 1. All the calculations were performed on three dimensional crystals consisting of primitive tetragonal lattice with 20 atoms. The energy conservation was achieved using 8^3 -points in the full Brillouin zone for sampling. Energy convergence criteria of 10^{-6} Ry were used for self-consistent calculations. The band structure is plotted along the path involving high symmetry points. The high

symmetry points for tetragonal lattice system in the first Brillouin zone are $\Gamma=(0,0,0)$, $X=(\frac{\pi}{a},0,0)$, $M=(\frac{\pi}{a},\frac{\pi}{a},0)$, $Z=(0,0,\frac{\pi}{c})$, $R=(\frac{\pi}{a},0,\frac{\pi}{c})$, $A=(\frac{\pi}{a},\frac{\pi}{a},\frac{\pi}{c})$. Calculated band structures were plotted along the high symmetry directions $\Gamma - X - M - \Gamma$, $Z - R - A - Z$, $X - R$, $M - A$.

IV. RESULTS AND DISCUSSION

In this study we have considered 4 canonical systems LaB_4 , CeB_4 , NdB_4 and SmB_4 with relatively small spin-orbit coupling strength and 4 canonical systems HoB_4 , ErB_4 , TmB_4 and LuB_4 with much larger spin-orbit coupling effect. In Table 1. we have summarized the lattice constants for systems under consideration. In Table 2. we have summarized the atomic spin-orbit coupling energy [25](in units of cm^{-1}) of various rare-earth atoms under consideration. It is important to mention that

Materials	a(Å)	c(Å)	Ecutwfc(Ry)	Ecutrho(Ry)
LaB_4	7.31066	4.18269	25	225
CeB_4	7.17377	4.07463	40	340
NdB_4	7.23842	4.11996	38	342
SmB_4	7.18656	4.08152	35	315
HoB_4	7.08619	4.00815	42	340
ErB_4	7.06973	3.99708	37	332
TmB_4	7.05321	3.98405	38	340
LuB_4	7.02687	3.96821	42	378

TABLE I: Lattice constants and the parameters used for the calculations.

Elements	SOC Energy(cm^{-1})	Elements	SOC Energy(cm^{-1})
La	5.6×10^3	Ho	8.1×10^3
Ce	5.8×10^3	Er	8.4×10^3
Nd	6.3×10^3	Tm	8.7×10^3
Sm	6.8×10^3	Lu	9.3×10^3

TABLE II: Tabulation for spin-orbit energy

Materials	Fermi energy $E_F(\text{eV})$	
	Without SOC	With SOC
LaB_4	12.447	12.523
CeB_4	13.103	13.103
NdB_4	12.290	12.303
SmB_4	12.285	12.301

TABLE III: Fermi Energy due to effect of low spin-orbit interaction materials.

the choice of kinetic energy cut-off and the number of k -points chosen over the irreducible Brillouin zone are extremely crucial in determining crystal structure and band structure calculation. We have calculated the total energy as a function of the plane wave kinetic energy

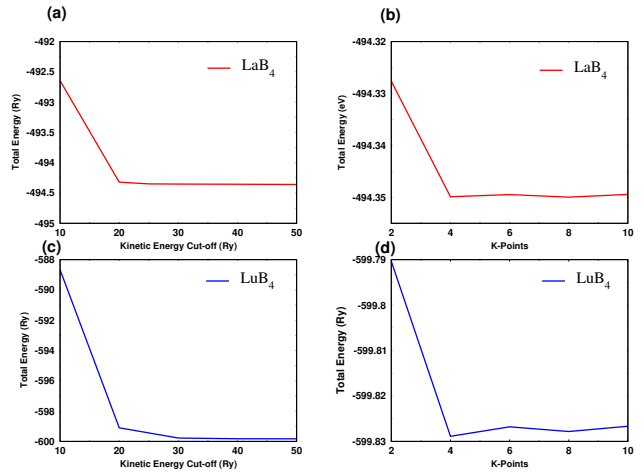


FIG. 2: Total Energy as a function of kinetic energy cut-off and k -points along irreducible edges. Convergence of self-consistent field for (a,b) LaB_4 and (c,d) LuB_4 , respectively.

cut-off as well as the number of k -points over irreducible Brillouin zone. In Fig. 2(a), (b) we show the convergence of the total energy as a function of kinetic cutoff and number of k -points for one canonical system LaB_4 with low spin-orbit coupling strength. In Fig. 2(c), (d) we have shown the same for LuB_4 , a material with much larger SOC strength. It is clear that the kinetic energy cut-off in the range of 20-50 Ry and 30-50 Ry are deemed to be sufficient for convergence of total energy in these two systems, respectively. Also, we have found that $4 \times 4 \times 4$ k -mesh (defined over irreducible Brillouin zone) is sufficient for relative stability of tetragonal structure. For the entire calculation we have chosen a k -mesh of size $8 \times 8 \times 8$.

A. Systems with low SOC effect

Taking the optimized crystal structure, we have calculated the electronic band structures and projected density of states (PDOS) with and without spin-orbit coupling effects under generalized gradient approximations (GGA) and GGA+SO, respectively. In Table 3. we compare Fermi energy for systems with and with out SOC. The Fermi energy for LaB_4 changes significantly but for other systems change is only at the second decimal place. The main reason is that except for LaB_4 (with SOC) the pseudo-potentials in the non-magnetic state does not involve highly localised $4f$ orbitals and SOC strongly affects $4f$ orbitals and its effect on other orbitals are only secondary through hybridization with $4f$ orbitals. In Fig. 3(a) we have shown the band structure for LaB_4 with and without SOC effect. The Fermi level is set to zero

for both the cases. As can be clearly observed from Fig. 3(a), (b) except at discrete symmetry points Γ , Z and R there is no significant SOC effect especially near the Fermi energy. However SOC lifts degeneracy at special symmetry points. Also, it can be observed that along the path $R - A$ bands are very flat and there is wide gap (of about 4 eV) between the top and bottom bands in this region. Flat bands correspond to non-dispersive localized bands arising mainly from deep core level state. In Fig. 4(a), (b) we have shown projected DOS from various orbitals at a given site in the absence of SOC. At the Fermi level the contribution is predominantly from B $2p$ and La $3d$. Discrete spectral peaks at -32 eV, -15 eV etc. arises due to deep core level states like B $1s$, La $1s$, $2p$. In Fig. 4(c) we show combined PDOS from all atoms as well as total DOS. When we switch on SOC the B $2p$ state gets split into two peaks corresponding to $j = 0.5$ and $j = 1.5$. Also La $3p$ state gets split into two peaks to $j = 0.5$ and $j = 1.5$. In the presence of SOC there is contribution of $4f$ state (split into $j = 2.5$ and $j = 3.5$) at the Fermi energy. This is a unique feature in the case of LaB_4 and is absent in all other systems we have considered in this study. PDOS corresponding to $4f$ is spread over wide range of energy from -10 eV to 7 eV but the total spectral weight is much smaller than B $2p$ and La $3d$ contributions. Just above the Fermi level, in the range 0 to 7.5 eV, PDOS arises due to strong hybridization between La $3d$ orbitals and B $1s$, $2p$ orbitals.

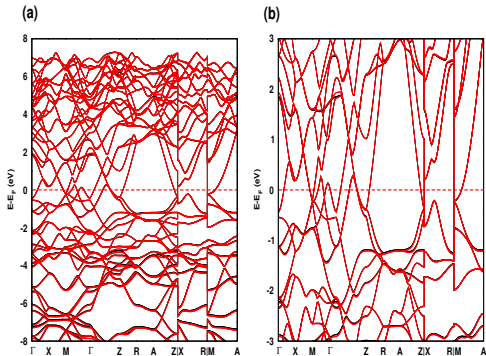


FIG. 3: (a) (Color online) Electronic band structure for LaB_4 . (a) represents band structure without (black) and with SOC (red). (b) represents same band structure in the narrower energy window about the Fermi level (set to zero).

In Fig. 5 we summarize the band structure and pro-

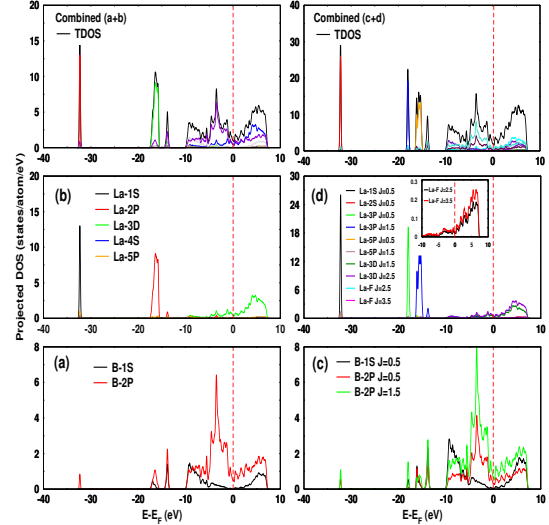


FIG. 4: (c) PDOS of LaB_4 in the absence of SOC. (a) and (b) shows contribution from different orbitals from B and La, respectively. Top left panel shows combined contribution from all orbitals. Discrete peaks at -32 eV, -17 eV arises mainly due to La $1s$ and La $2p$ orbitals while the peak at -15 eV due to B $2p$. (c) and (d) shows spin-split contribution from various B and La orbitals in the presence of SOC. The peak at -17 eV gets split into two peaks with $j = 0.5$ and $j = 1.5$. Inset of (d) shows contribution of spin-split $4f$ orbitals about Fermi level. Top right panel shows the combined contribution from all orbitals.

jected density of states of CeB_4 with and without SOC effects. Ce is the first atom in the lanthanides series which contains $4f$ orbital. As can be clearly seen from Fig. 5(a) and 5(b) in the presence of SOC, otherwise degenerate bands split at Γ and R points but the bands remain degenerate at Z point. As in the case of LaB_4 there exists non-dispersive flat bands along $R - A - Z$ directions and there is a gap of around 4.5 eV between the top and the bottom bands. In Fig. 5(c) we show the PDOS arising from various atomic orbitals in the absence of SOC effects. The distinct spectral peaks appearing at -14 eV and at -17 eV are due to B $2p$ and Ce $3p$ orbitals, respectively. The extremely narrow spectral peak at -34 eV arises due to deep core level Ce $1s$ state and B $2p$. The continuum density of states in the energy window -10 eV to 8 eV arises due to hybridized B $2p$ and Ce $3p$, Ce $4p$, Ce $5d$ orbitals. In Fig. 5(d) we show the effect of SOC on PDOS for various atoms. As in the case of LaB_4 there is appearance of extremely narrow peak at -19 eV due to splitting of spin-degenerate B $2p$ and Ce $3p$ orbitals into $j = 0.5$ and $j = 1.5$ manifolds. The DOS in the energy window -10 eV to 8 eV remains largely unaffected as in the case of LaB_4 and there is no additional

contribution due to spin split Ce 4*f* orbitals.

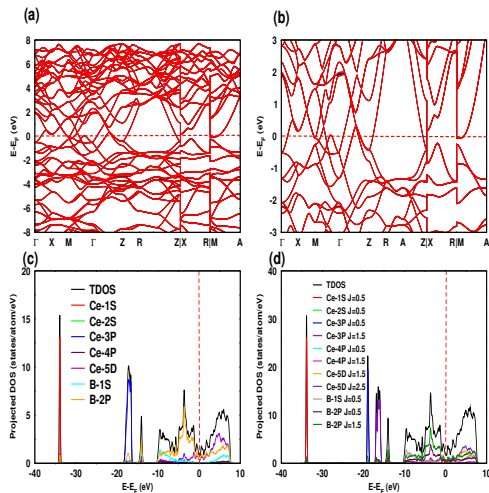


FIG. 5: (a) (Color online) Combined Band structure of CeB_4 with out (black) and with SOC (red), (b) same band structure in the narrower energy window about the Fermi level (set to zero). Degenerate band splits at Γ and R points. Fig. (c) and (d) The PDOS of CeB_4 . The distinct spectral peaks appearing at -14 eV and at -17 eV are due to B 2*p* and Ce 3*p* orbitals, respectively. In the energy window -10 eV to 8 eV represents continuum DOS due to hybridized B 2*p* and Ce 3*p*, Ce 4*p*, Ce 5*d* orbitals.

The band structure and projected density of states of NdB_4 with and without SOC effects have been summarised in Fig. 6. As shown in Fig. 6(a) and 6(b), the spin degenerate bands splits in various regions due to SOC effects present in these systems. Band splitting is more explicit along the direction $\Gamma - Z - R$ and $A - Z$. Very few bands cross the Fermi level and far from Fermi level most of the bands are much less dispersed and nearly flat. In Fig. 6(c) we show the PDOS from various atoms without SOC effects. As in the earlier cases the distinct spectral peak at -15 eV arises due to B 2*p* orbitals and the spectral peak at -19.5 eV arises due to B 2*p* and Nd 3*p* orbitals, respectively. The extremely narrow spectral peak at -38 eV arises mainly due to non-dispersive deep core-level Nd 1*s* orbital. However B 2*p* orbitals have also contribution towards the peak at -38 eV. The continuum density of states in the energy range between -10.5 eV to 7.5 eV arises due to hybridized B 2*p* and Nd 3*p*, Nd 4*p*, Nd 5*d* orbitals. Finally, in Fig. 6(d) we show the PDOS in the presence of SOC effect. The continuum DOS in the range -10.5 eV to 7.5 eV remains largely unaffected. However the peak at -19.5 eV gets split into two peaks at -18 eV and -21 eV. This arises due to otherwise degenerate B 2*p* and Nd 3*p* orbitals splitting into $j = 0.5$ and

$j = 1.5$ manifolds due to SOC effects.

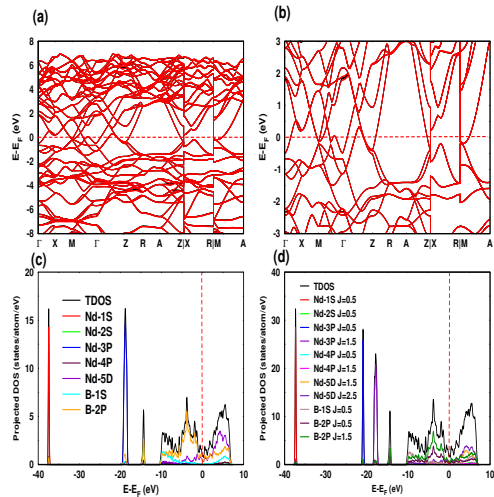


FIG. 6: (a) (color online) Combined Band structure of NdB_4 with out (black) and with (red) SOC, (b) same band structure in the narrower energy window about Fermi level (set to zero). Fig. (c) and (d) The PDOS of NdB_4 . Very small narrow spectral peak at -38 eV is found due to non-dispersive deep core-level Nd 1*s* orbital. Other peaks at -38 eV arises for B 2*p* orbitals. The continuum DOS in the energy range between -10.5 eV to 7.5 eV arises due to hybridized B 2*p* and Nd 3*p*, Nd 4*p*, Nd 5*d* orbitals.

In Fig. 7 represents the band structure and density of states of SmB_4 with and without SOC effects. It is interesting to mention that SmB_4 is metallic whereas SmB_6 is a Kondo insulator where Sm shows mixed valency Sm^{+2} and Sm^{+3} at the ratio 3:7. In Fig. 7(a) and 7(b) we show electronic band structure. Splitting of energy bands in the $\Gamma - Z - R$ direction is much more prominent due to much larger SOC effects. Energy bands along $R - A - Z$ continues to remain flat. In Fig. 7(c) we show PDOS. The discrete peak arising due to Sm 1*s* shifts further down to -41 eV. The spectral peak at -20.5 eV and -14.5 eV arises due to B 2*p*, Sm 3*p* and B 1*s*, 2*p* orbitals, respectively. The origin of continuum states in the range -10.5 eV to 8 eV is same as earlier. When we switch on the SOC the spectral peak arising due to *p*-orbitals of B and Sm gets split into $j = 0.5$ and $j = 1.5$ states and the corresponding spectral peaks appears at -23 eV and -19 eV, respectively.

B. Systems with large SOC Effect

In the previous section we have considered SOC effects on 4 canonical systems with relatively low SOC effect.

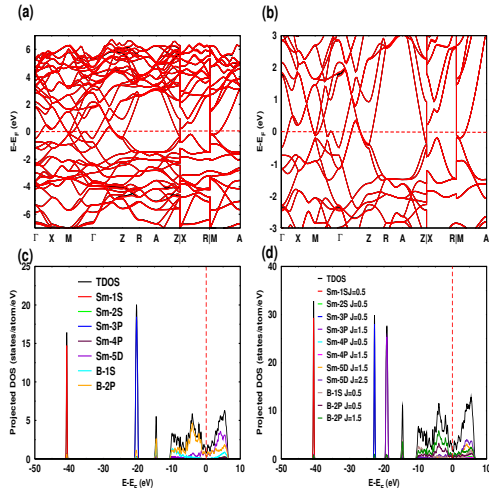


FIG. 7: (a) (color online) Combined Band structure of SmB_4 with out (black) and with (red) SOC, (b) same band structure in the narrower energy window about the Fermi level (set to zero). Fig. (c) and (d) the PDOS of SmB_4 . The isolated spectral peak at -20.5 eV and -14.5 eV corresponds to B $2p$, Sm $3p$ and B $1s$, $2p$ orbitals, respectively.

In this section we consider SOC effects on 4 canonical systems with relatively large SOC effects. In Table. IV we have summarized the Fermi energy with and without SOC effects.

In Fig. 8 we have shown the band structure and projected DOS for HoB_4 with and without SOC effects. SOC effects on the splitting of energy bands are prominent for wide range of energies. Bands far away from Fermi energy are also affected due to strong SOC effects. Degeneracy lifting effect along $\Gamma - Z - R$ are now quite explicit. Fermi level crossing bands along $Z - R$ are also affected. However flat bands along $R - A - Z$ are not affected by SOC. In Fig. 8(c) we show PDOS due to various atoms as earlier. Continuum DOS in the range -10.5 eV to 7.5 eV arises due to strong hybridization between $5d$ orbitals of Ho and $2p$ orbitals of B atoms. The spectral peak at -14 eV arises due to $2p$ orbitals of B atoms while the peak at -24 eV arises due to Ho $3p$ orbitals. Extremely narrow and isolated peak at -48 eV arises due to deep core level $1s$ orbital of Ho atom. In Fig. 8(d) we show the effect of SOC on PDOS. There is enhancement of PDOS around Fermi level. The spectral peak at -24 eV gets split into two peaks at -27 eV and -22 eV which arises due to Ho orbitals with $j = 0.5$ and $j = 1.5$, respectively.

Fig. 9 indicates the band structure and projected density of states of ErB_4 in the presence and absence of SOC effects. As seen in Fig. 9(a) and 9(b), spin-split bands are quite visible in the energy range -4 eV to -6 eV along

Materials	Fermi energy E_F (eV)	
	Without SOC	With SOC
HoB_4	12.271	12.279
ErB_4	12.280	12.286
TmB_4	12.274	12.278
LuB_4	12.251	12.251

TABLE IV: Fermi Energy due to effect of large spin-orbit interaction materials.

$\Gamma - Z - R$ direction. Band splitting effects near the Fermi level also starts showing up. Projected density of states as shown in Fig. 9(c) follows similar trend as in the case of other tetra-borides. The continuum density of states in the range -10 eV to 7 eV arises from the hybridized B $2p$ and Er $5d$ orbitals. The spectral peak due to Er $1s$ is now at -51 eV. While the Er $3p + B 2p$ spectral peak is at -25 eV. The smaller peak arising due to B $2p$ is at -15 eV. As shown in Fig. 9(d), inclusion of SOC effect causes splitting of the -25 eV peak into $j = 0.5$ and $j = 1.5$ states situated at -29 eV and -23.5 eV, respectively.

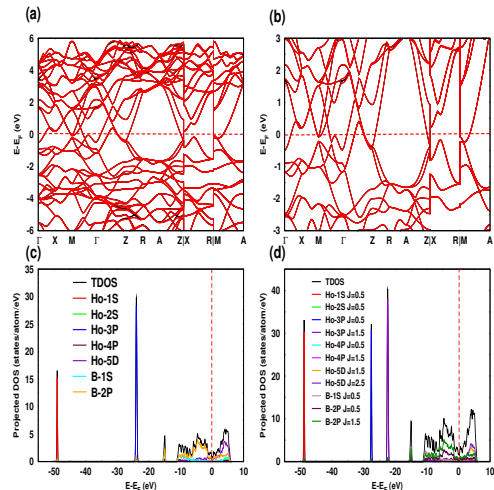


FIG. 8: (a) (Color online) Combined Band structure of HoB_4 without (black) and with (red) SOC, (b) same band structure in the narrower energy window about the Fermi level. The spectral peak at -14 eV corresponds to $2p$ orbitals of B atoms while the peak at -24 eV arises due to Ho $3p$ orbitals. Extremely narrow and isolated peak is found at -48 eV due to deep core level $1s$ orbital of Ho atom. Fig. (c) and (d) The PDOS of HoB_4 . Showing the individual contributions from each orbital atom with and without SOC effect. The Fermi energy is set to zero assigned by the dotted red line.

In Fig. 10 we summarize the electronic band structure

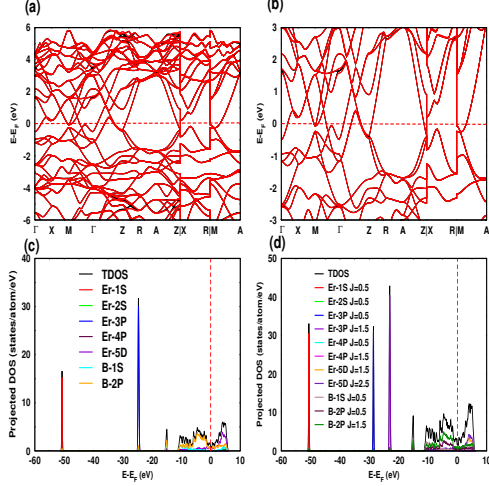


FIG. 9: (a) (Color online) Combined Band structure of ErB_4 with (red) and without SOC (black), (b) same band structure in the narrower energy window about the Fermi level (set to zero). The spin-split bands appearing in the energy range -4 eV to -6 eV along $\Gamma - Z - R$ direction. (c) and (d) PDOS of ErB_4 . The spectral peak due to Er $1s$ is now at -51 eV. While the Er $3p + B 2p$ spectral peak is at -25 eV. At -15 eV due to B $2p$ orbital. (d) Inclusion of SOC effect causes splitting of the -25 eV peak into $j = 0.5$ and $j = 1.5$ states situated at -29 eV and -23.5 eV, respectively

and projected density of states of TmB_4 . In an earlier study band structure for TmB_4 in the anti-ferromagnetic state was reported. So the present study is relevant in the paramagnetic state of this system. As shown in Fig. 10(a) and 10(b) energy bands far from the Fermi level are strongly affected due to SOC. Energy bands in the energy range -4 eV to -6 eV show significant splitting especially along $\Gamma - Z - R$ direction. Similar features are also observable for energy bands in the window 1 eV to 2 eV. Some of the Fermi level crossing bands show degeneracy lifting effects near Fermi level. The spectral features are similar to the other tetraborides. The peaks arising due to Tm $1s$, $3p$ and B $2p$ are at -52.5 eV and -26 eV respectively. The continuum DOS in the energy range -11 eV to 7 eV arises due to hybridized Tm $4p$, $5d$ orbitals with B $2p$ orbitals. Inclusion of SOC, as shown in Fig. 10(d), causes splitting of the -26 eV spectral peaks into a $j = 0.5$ peak at -30 eV and a $j = 1.5$ peak at -24 eV.

Finally, in Fig. 11 we show our results for LuB_4 . Incidentally Lu is the last member of the lanthanide series with completely filled $4f$ orbitals. As in the case of TmB_4 there is strong SOC effects on the energy bands in the energy window -6 eV to -4 eV as well as in the window 1 eV

to 2 eV. SOC effects on the Fermi level crossing bands near Fermi energy are less compared to TmB_4 . These features are well summarised in Fig. 11(a) and 11(b). In Fig. 11(c) and 11(d) we show the projected DOS in the absence and presence of SOC effects, respectively. The spectral peak at -56 eV is due to Lu $1s$ orbital while the peak at -15 eV is due to B $1s$ and $2p$. There is a strong peak at -27 eV arising due to Lu $3p$ orbital. The height of this peak is much more than the other two discrete peaks. The continuum of density of states around Fermi level arises due to hybridized B $2p$ and Lu $5d$ orbitals. In the presence of SOC the peak at -26 eV gets split onto two peaks at -32 eV and -25 eV with $j = 0.5$ and $j = 1.5$, respectively.

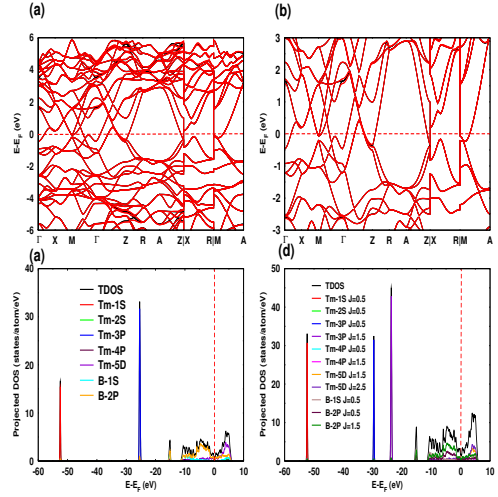


FIG. 10: (a) (color online) Combined Band structure of TmB_4 without (black) and with (red) SOC, (b) same band structure in the narrower energy window about Fermi level (set to zero). Fig. (c) and (d) The PDOS of TmB_4 . Showing the individual contributions from each orbital atom with and without SOC effect. The continuum DOS in the energy range -11 eV to 7 eV arises due to hybridized Tm $4p$, $5d$ orbitals with B $2p$ orbitals. With SOC, the p-orbital split into a $j = 0.5$ peak at -30 eV and a $j = 1.5$ peak at -24 eV.

V. CONCLUSION

We have investigated the electronic structure of RB_4 with non-magnetic ground state. The electronic band structure shows splitting due to interaction between spin and angular momentum. The bands splitting has been interpreted with the help of PDOS. It has also been observed that the two new branches for p-orbital appearing due to SOC effect. In case of LaB_4 with SOC,

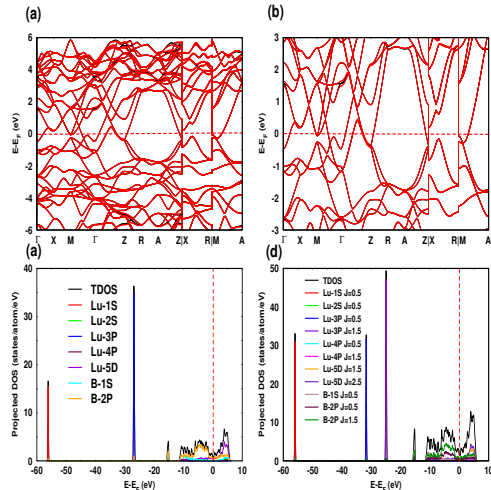


FIG. 11: (a) (color online) Combined Band structure of LuB₄ without (black) and with (red) SOC, (b) same band structure in the narrower energy window about Fermi level (indicates dotted red line). Fig. (c) and (d) The PDOS of LuB₄. In the presence of SOC the peak at -26 eV gets split onto two peaks at -32 eV and -25 eV with $j = 0.5$ and $j = 1.5$, respectively like other system.

the contribution of $4f$ orbitals to the DOS about the Fermi level has been observed. This work is partially supported by WB- DSTBT research grant no. STBT-11012(26)/31/2019-ST SEC. One of us (NP) would like to acknowledge hospitality of IIT, Kharagpore. One of us (IS) would like to thank Bajkul Milani Mahavidyalaya (College) authority for giving me an opportunity to pursue research as a Ph. D. scholar.

- ¹ Goryachev, Y.M., Kovenskaya, B.A., Dudnik, E.M. et al. Electronic structure of tetraborides of the rare earth elements. *J Struct Chem* **16**, 951–954 (1975).
- ² Felix Frontini et al. Intermediate valence state in YbB₄ revealed by resonant x-ray emission spectroscopy. *J. Phys.: Condens. Matter* **34** 34560 (2022)
- ³ ai Swaroop Sunku, Tai Kong, Toshimitsu Ito, Paul C.Canfield, B. Sriram Shastry, Pinaki Sengupta, and Christos Panagopoulos, *Phys. Rev. B* **93**, 174408 (2016)
- ⁴ Nandan Pakhira, Jyoti Krishna, S. Nandy, T. Maitra, and A Taraphder. Electronic structure of metallic tetra-boride TmB₄: An LDA+DMFT study.arXiv:1807.05388
- ⁵ B. S. Shastry and B. Sutherland :Exact ground state of a quantum mechanical antiferromagnet. *Physica B* **108** 1069(1981)
- ⁶ Miyahara, S. Ueda, K. Theory of the orthogonal dimer Heisenberg spin model for SrCu₂(BO₃)₂. *J. Physics: Condens. Matter* **15**, R327 (2003).
- ⁷ Lawrence Baylor Robinson, Lloyd N. Ferguson, Jr., and Frederick Milstein. Indirect Exchange Coupling of Magnetic Moments in Rare-Earth Metals. *Phys. Rev. B* **3**, 1025-1033 (1971)
- ⁸ T. Mtasumurai, D.Okuyama, T. Mouri, and Y. Murakami *J. Phys. Soc. Jpn* **80**, 074701 (2011)
- ⁹ Pradhan, Subhasree and A. Taraphder. “First-Principles Study of The Metallic Rare-Earth Tetraboride TmB₄.” *Materials Today: Proceedings* **4** (2017): 5532-5536.
- ¹⁰ Z. P. Yin and W. E. Pickett, Rare-earth–boron bonding and $4f$ state trends in RB₄ tetraborides.*Physical Review B* **77**, 035135 2008
- ¹¹ Choi, Hongchul and Laref, Amel and Shim, Ji and Kwon, S. and Min, B.(2009). Electronic structures and magnetic properties of RB₄ (R=Yb,Pr,Gd,Tb,Dy). *Journal of Applied Physics*. **105**. 07E107 - 07E107. 10.1063/1.3058707.
- ¹² Olsen, J. Wařkowska, A. Gerward, L. Vaitheeswaran, Ganapathy Venkatakrishnan, Kanchana Svane, A. Shitsevalova, Natalya Phillipov, V.. (2011). HoB₄ at high pressure and low temperature: An experimental and theoretical study. *High Pressure Research*. **31**. 3-6. 10.1080/08957959.2010.513683.
- ¹³ Z. Fisk and M. B. Maple, Multiple Phase Transition in Rare Earth Tetraborides at Low Temperature. *Solid State Commun.* **39**, 1189 1981.
- ¹⁴ WILL, G. and SCHFER, W.. ”The crystal structures of ErB₄ and DyB₄ studied by neutron diffraction” *Zeitschrift fr Kristallographie - Crystalline Materials* **144**, 217-225 (1976)
- ¹⁵ P. Hohenberg and W. Kohn *Phys. Rev.* **136**, B864 (1964).
- ¹⁶ W. Kohn and L.J. Sham, *Phys. Rev.* **140**, A1133 (1965).
- ¹⁷ Paolo Giannozzi et al. QUANTUM ESPRESSO: a modular and open-source software project for quantum simulations of materials. *J. Phys.: Condens. Matter* **21** 395502 (2009)
- ¹⁸ <https://nisihara.wixsite.com/burai/>
- ¹⁹ Vanderbilt David. Soft self-consistent pseudopotentials in a generalized eigenvalue formalism. *Phys. Rev. B* **41**, 7892–7897 (1990)
- ²⁰ N. Marzari, D. Vanderbilt, A. De Vita, and M. C. Payne, “Thermal contraction and disordering of the Al(110) sur-

- face,” *Phys. Rev. Lett.* **82**, 3296–3299 (1999).
- ²¹ Perdew, J. P., Zunger, Alex. Self-interaction correction to density-functional approximations for many-electron systems. *Phys. Rev. B* **23**, 5048 (1981)
- ²² Baroni, Stefano and de Gironcoli, Stefano and Dal Corso, Andrea and Giannozzi, Paolo. Phonons and related crystal properties from density-functional perturbation theory. *Rev. Mod. Phys.* **73**, 515-520(2001)
- ²³ Islam, M.R., Islam, M.S., Ferdous, N. et al. Spin-orbit coupling effects on the electronic structure of two-dimensional silicon carbide. *J Comput Electron* **18**, 407–414 (2019).
- ²⁴ A. Jain, S.P. Ong, G. Hautier, et al. The Materials Project: A materials genome approach to accelerating materials innovation *APL Materials*, 2013, **1**(1), 011002.
- ²⁵ Martin WC. Table of Spin-Orbit Energies for p-Electrons in Neutral Atomic (core)np Configurations. *J Res Natl Bur Stand A Phys Chem.* 1971; **75A**(2):109-111. doi:10.6028/jres.075A.010